
AFRL-ML-WP-TP-2007-537

# ELECTRICAL, STRUCTURAL, AND OPTICAL PROPERTIES OF CR-DOPED AND NON-STOICHIOMETRIC $V_2O_3$ THIN FILMS (PREPRINT)

**Patricia A. Metcalf, Leonel P. Gonzalez, Jacob O. Barnes, Elliott Slamovich, Shekhar Guha, and Jurgen M. Honig**

**Hardened Materials Branch**
**Survivability and Sensor Materials Division**

**JUNE 2006**



**AIR FORCE RESEARCH LABORATORY**
**MATERIALS AND MANUFACTURING DIRECTORATE**
**WRIGHT-PATTERSON AIR FORCE BASE, OH 45433-7750**
**AIR FORCE MATERIEL COMMAND**
**UNITED STATES AIR FORCE**

# NOTICE AND SIGNATURE PAGE



AFRL-ML-WP-TP-2007-537 HAS BEEN REVIEWED AND IS APPROVED FOR PUBLICATION IN ACCORDANCE WITH ASSIGNED DISTRIBUTION STATEMENT.

*//Signature//

SHEKHAR GUHA, Ph.D.
Agile IR Limiters
Exploratory Development
Hardened Materials Branch

//Signature//

MARK S. FORTE, Acting Chief
Hardened Materials Branch
Survivability and Sensor Materials Division

//Signature//

TIM J. SCHUMACHER, Chief
Survivability and Sensor Materials Division

This report is published in the interest of scientific and technical information exchange, and its publication does not constitute the Government's approval or disapproval of its ideas or findings.

*Disseminated copies will show "//Signature//" stamped or typed above the signature blocks.

# REPORT DOCUMENTATION PAGE

*Form Approved*
*OMB No. 0704-0188*



| 1. REPORT DATE *(DD-MM-YY)* | 2. REPORT TYPE | 3. DATES COVERED *(From - To)* |
|---|---|---|
| June 2006 | Journal Article Preprint | |

**4. TITLE AND SUBTITLE**

ELECTRICAL, STRUCTURAL, AND OPTICAL PROPERTIES OF CR-DOPED AND NON-STOICHIOMETRIC $V_2O_3$ THIN FILMS (PREPRINT)

**5a. CONTRACT NUMBER**
In-house

**5b. GRANT NUMBER**

**5c. PROGRAM ELEMENT NUMBER**
62102F

**6. AUTHOR(S)**

Patricia A. Metcalf, Elliott Slamovich, and Jurgen M. Honig (Purdue University)
Leonel P. Gonzalez and Jacob O. Barnes (General Dynamics Information Technology, Inc.)
Shekhar Guha (AFRL/MLPJ)

**5d. PROJECT NUMBER**
4348

**5e. TASK NUMBER**
RG

**5f. WORK UNIT NUMBER**
M08R1000

**7. PERFORMING ORGANIZATION NAME(S) AND ADDRESS(ES)**

Purdue University
West Lafayette, IN

General Dynamics Information Technology, Inc.
5100 Springfield Pike, Suite 509
Dayton, OH 45431-1264

Hardened Materials Branch (AFRL/MLPJ)
Survivability and Sensor Materials Division
Materials and Manufacturing Directorate
Wright-Patterson Air Force Base, OH 45433-7750
Air Force Materiel Command, United States Air Force

**8. PERFORMING ORGANIZATION REPORT NUMBER**
AFRL-ML-WP-TP-2007-537

**9. SPONSORING/MONITORING AGENCY NAME(S) AND ADDRESS(ES)**

Air Force Research Laboratory
Materials and Manufacturing Directorate
Wright-Patterson Air Force Base, OH 45433-7750
Air Force Materiel Command
United States Air Force

**10. SPONSORING/MONITORING AGENCY ACRONYM(S)**
AFRL/MLPJ

**11. SPONSORING/MONITORING AGENCY REPORT NUMBER(S)**
AFRL-ML-WP-TP-2007-537

**12. DISTRIBUTION/AVAILABILITY STATEMENT**
Approved for public release; distribution unlimited.

**13. SUPPLEMENTARY NOTES**
Journal article submitted to Thin Solid Films.



**14. ABSTRACT**

$V_2O_3$ films and Cr-doped $V_2O_3$ films were grown on (0001) (C-plane) and (1120) (plane) oriented sapphire substrates by the reduction of sol-gel derived vanadium oxide films. Examination by x-ray diffraction, SEM, TEM, and atomic force microscopy showed the films to be comprised of highly oriented grains. Optical transmission and dc resistivity measurements revealed phase transitions characteristic of the single crystal $V_2O_3$ and Cr-doped $V_2O_3$. Subsequent anneals of the un-doped films under controlled oxygen atmospheres yielded non-stoichiometric films with metal-insulator transitions characteristic of annealed $V_2O_3$ single crystals.

**15. SUBJECT TERMS**
Phase Transitions, Vanadium Oxide, Optical Properties, Electrical Properties

| 16. SECURITY CLASSIFICATION OF: | | | 17. LIMITATION OF ABSTRACT: | 18. NUMBER OF PAGES | 19a. NAME OF RESPONSIBLE PERSON (Monitor) |
|---|---|---|---|---|---|
| a. REPORT | b. ABSTRACT | c. THIS PAGE | | | Shekhar Guha |
| Unclassified | Unclassified | Unclassified | SAR | 26 | 19b. TELEPHONE NUMBER *(Include Area Code)* N/A |

**Standard Form 298 (Rev. 8-98)**
Prescribed by ANSI Std. Z39-18

# Electrical, Structural, and Optical Properties of Cr-doped and Non- stoichiometric $V_2O_3$ Thin Films

**Patricia A. Metcalf,[a*] Leonel P. Gonzalez,[b] Jacob O. Barnes,[b] Elliott Slamovich,[a] Shekhar Guha[c] and Jurgen M. Honig[d]**

*[a]Materials Engineering, [d]Department of Chemistry, Purdue University, West Lafayette, Indiana, USA; [b]Materials and Manufacturing Directorate, Anteon Corp., Dayton, Ohio, USA; [c]Materials and Manufacturing Directorate, Air Force Research Laboratory, Wright Patterson AFB, Ohio, USA*

*Corresponding author: metcalfp@purdue.edu

## Abstract

$V_2O_3$ films and Cr-doped $V_2O_3$ films were grown on (0001) (C-plane) and (1120) (plane) oriented sapphire substrates by the reduction of sol-gel derived vanadium oxide films. Examination by x-ray diffraction, SEM, TEM, and atomic force microscopy showed the films to be comprised of highly oriented grains. Optical transmission and dc resistivity measurements revealed phase transitions characteristic of the single crystal $V_2O_3$ and Cr-doped $V_2O_3$. Subsequent anneals of the un-doped films under controlled oxygen atmospheres yielded non-stoichiometric films with metal-insulator transitions characteristic of annealed $V_2O_3$ single crystals.

*Keywords:* Phase transitions; Vanadium oxide; Optical properties; Electrical properties

## 1. Introduction

A variety of crystal phases exist in the vanadium-oxygen system, a number of which display dramatic changes in electronic, magnetic, and optical properties associated with phase transitions. Among the most interesting and widely studied is vanadium sesquioxide, $V_2O_3$, which upon cooling from room temperature exhibits a paramagnetic metal (PM) to antiferromagnetic insulator (AFI) phase transition at about 150 K. The metal-insulator transition temperature in $V_2O_3$ is sensitive to applied pressure, vanadium to oxygen ratio, and dopant concentration with elements like Cr and Ti [1-7]. For single crystal $V_{2-y}O_3$, the metal-insulator transition temperature decreases with an increase in oxygen excess. In $(V_{1-x}Cr_x)_2O_3$, with chromium doping of $x < 0.005$, the PM to AFI insulator transition temperature increases slightly with increasing chromium concentration. In addition, $(V_{1-x}Cr_x)_2O_3$ samples doped with chromium ($0.005 < x < 0.018$) exhibit a paramagnetic metal (PM) to paramagnetic insulator (PI) phase transition at higher temperature. The crystal structure of $V_2O_3$ is rhombohedral in the PM and PI phases and monoclinic in the AFI phase. The phase transition is accompanied by a cell volume change, causing crystals to fracture when thermally cycled [8]. A generalized phase diagram for $V_2O_3$ as a function of temperature and chromium dopant concentration, at 1 atm. pressure, is shown in Figure 1. The phase diagram was determined from measurements of single crystal $(V_{1-x}Cr_x)_2O_3$ samples and controlled atmosphere annealed $V_{2-2y}O_3$ samples [1,6]. Since a hysteresis effect is encountered in resistivity measurements across the phase transition in crystals, this phase diagram depicts the results of measurements

taken upon sample cooling.

In the past ten years, there have been a number of reports on the growth of thin films [9-16] and ultra-thin films [17-27] of $V_2O_3$ by reactive sputtering, reactive evaporation, pulsed laser deposition, and the sol-gel technique. By contrast, there are only two reports on the growth of Cr-doped $V_2O_3$ thin films [28, 29], and no reports on systematically prepared non-stoichiometric $V_2O_3$ thin films. Schuler *et. al*. [12] reported that for $V_2O_3$ films grown epitaxially on (0001) oriented sapphire substrates by reactive evaporation, the transition is broadened by the strain induced by lattice mismatch. It was proposed that the substrate-film interaction hinders the structural transition from the rhombohedral to monoclinic lattice. For ultra-thin films, less than 30 nm in thickness [23], the MIT is completely suppressed by the substrate-film interaction.

Although a substantial amount of work has been done on the effects on the electronic transition of doping single crystal $V_2O_3$ with chromium [1,6], little has been reported for chromium doped $V_2O_3$ films. Greenberg and Singleton [28] reported that for sol-gel derived chromium doped thin films, the conductivity "tended toward insulating" with increased chromium concentration. Based on dc resistivity measurements, Piao *et al*. [29] reported an increase in the transition temperature with increasing chromium concentration, but attributed the absence of the higher temperature PM to PI transition to the small grain size in the sol-gel derived films.

## 2. Experiment

$V_2O_3$ films were synthesized by heat-treating sol-gel derived vanadium oxide films in reducing atmospheres. The sol-gel films were prepared by spin-coating a solution of vanadium triisopropoxide, $VO(PrO)_3$, in isopropanol onto single crystalline, polished (0 0 0 1) (C-plane) and (1 1 $\bar{2}$ 0) (A-plane) oriented sapphire substrates. Sol-gel films were formed by the hydrolysis and condensation of neutral precursors in the ambient humidity. The films were dried at 85°C, and the procedure was repeated to form one to nine layers. Chromium doped films were prepared by dissolving the chloride or acetylacetonate salts into isopropanol prior to the addition of the alkoxide. The amorphous, as-deposited films were then heat-treated in reducing atmospheres to obtain crystalline, 125 nm to 1250 nm thick $V_2O_3$ films. The vanadium oxide phases present in the annealed films were depended on both the annealing atmosphere and temperature. $V_2O_3$ films were formed by heating the sol-gel films in a 5% hydrogen – 95% argon gas mixture at 850°C for two hours. The non-stoichimetric films were prepared by subsequent annealing of the $V_2O_3$ films in a vertical quench annealing furnace equipped with an oxygen sensor. The operational details of this system have been described elsewhere [30].

The resulting films were examined by x-ray diffraction (XRD) utilizing a Cu K$\alpha$ radiation source, scanning electron microscopy (SEM), transmission electron microscopy (TEM), and atomic force microscopy (AFM). The electrical resistance was measured using a standard four-probe technique. The optical transmission

measurements were performed using a Perkin Elmer Spectrum-GX FTIR Spectrometer.

## 3. Results and Discussion

### 3.1. X-ray Diffraction and Microscopy

The X-ray diffraction patterns of 300 nm thick $V_2O_3$ films deposited on (0001) and (1120) oriented sapphire substrates are presented in Figures 2a and 2b. The results suggest that the films assume a preferred *c-axis* orientation on (0001) oriented sapphire substrates and a preferred *a-axis* orientation on (1120) oriented sapphire substrates. The X-ray diffraction patterns for films with thickness greater than 600 nm show the presence of other orientations, indicating a loss of preferred orientation in thicker films.

Observation of the surface of a $V_2O_3$ film on sapphire by Scanning Electron Microscopy indicated that the film surfaces are relatively smooth. Crystallites from $V_2O_3$ thin film grown on C-sapphire at 925°C are shown in Figure 3. The sapphire substrate was ground from the reverse side, and the film was examined by Transmission Electron Microscopy. The $V_2O_3$ crystallites vary from 60 to 300 nm in diameter and are embedded in an amorphous matrix.

The surface morphology of a 300 nm thick $V_2O_3$ film on a (0001) oriented sapphire substrate is shown in the atomic force microscope images in Figure 4. The images were obtained using a non-contact mode. The scan area in image (a) is 1μ x 1μ and that in image (b) is 500 nm x 500 nm. The $V_2O_3$ film, which was annealed for two hours at 850°C, consists of grains oriented along the c-direction,

consistent with the PXD results. The average grain size is about 60 nm, with a surface roughness of about 15 nm. An increase in temperature or annealing time resulted in an increase in grain size and surface roughness.

### 3.2. Optical and Electronic Properties

In Figures 5a and 5b, plots of the electrical resistivity measured as a function of temperature are shown for $V_2O_3$ films on C and A-sapphire substrates. The metal-insulator transition occurs at a temperature of about 150 K in both films. Figure 5c shows the metal-insulator transition for a single crystal of $V_{2-2y}O_3$, y = 0.000, grown and annealed at Purdue University. The transition is slightly broadened in the films compared with the single crystal, and displays a temperature hysteresis of about 20 K. Transition broadening has been seen for other $V_2O_3$ films [9-16], and attributed to the strain induced by lattice mismatch. The change in resistivity at the transition temperature is about eight orders of magnitude for the single crystal, while it is about six in the films. These measurements suggest that the films are stoichiometric and that the electrical properties of the films do not differ greatly from those of the bulk material.

The optical transmittance of a $V_2O_3$ film on C-sapphire and A-sapphire recorded at temperatures above and below the phase transition in presented in Figure 6. The figure shows the switching of the optical transmission from about 40% at 5 microns near room temperature to about 80% at 77 K. This is consistent with the existence of an electrical transition in the $V_2O_3$ films from a metal at room temperature, to an insulator below the 150 K transition. The value of the room

temperature transmission is dependent upon the thickness of the film.

The electrical conductivity versus temperature for several $(V_{1-x}Cr_x)_2O_3$ films is given in figure 7a. Presented for reference, figure 7b is a plot, extracted from reference 6, depicting the changes in the electrical conductivity of chromium doped $V_2O_3$ crystals as a function of temperature. It can be seen that the metal-insulator phase transition is present in chromium doped $V_2O_3$ films, and that their electrical properties do not differ greatly from those found in single crystals. As in the un-doped films, the transitions are somewhat broader and the magnitude of the transitions is less than is seen in the single crystal samples.

The optical transmittance of $(V_{1-x}Cr_x)_2O_3$ films on C-sapphire as a function of temperature is presented in Figure 8. The un-doped film shows a transition at 150 K from a metal with a transmission of about 7% to an insulator with a transmission of about 60%. Referring to the single crystal behavior presented in Figure 7b, the films show a similar behavior with an increase in the low temperature metal-insulator transition temperature with increasing chromium concentration. The higher temperature transition appears in the optical transmission measurement. It is also broadened and reduced in magnitude relative to measurements on single crystals.

Figure 9 is a plot of the optical transmission at 4 micron versus temperature for annealed, non-stoichimetric $V_{2-y}O_3$ films. As referenced in Figure 1, the metal-insulator transition temperature decreases with increasing non-stoichiometry. The values for y given in Figure 9 have been extrapolated from transition temperatures

for the data on single crystals from reference 7. The transitions are again very broad and decreased in amplitude. In addition, it was found that to obtain the same transition temperature, and degree of non-stoichiometry, the films must be annealed at much lower oxygen pressures than for the single crystals. It is possible that a small amount of re-oxidation occurs during the quench, which is insignificant in the bulk crystals, but is significant for the small grains in the films. From figure 1, it can be seen that below y=0.012, the transitions occur below the 77 K temperature limit of the optical measurements.

## 4. Conclusions

Films with thicknesses from 125 nm to 1250 nm of $V_2O_3$ and chromium doped $V_2O_3$ films on sapphire substrates have been successfully grown using the sol-gel method. The un-doped films were subsequently annealed under controlled oxygen atmospheres. Examination by PXD, SEM, TEM and AFM revealed that the films were comprised of well-formed, highly oriented grains. Optical transmission and dc-resistivity measurements revealed that the films undergo phase transitions similar to those of single crystals. In comparison with the known phase diagram for the single crystal $V_{2-y}O_3$ and $(V_{1-x}Cr_x)_2O_3$ system, it can be seen that the films exhibit a similar phase relationship. The PM to AFI transition temperature decreases from about 150 K as the vanadium to oxygen ratio is changed by annealing. The PM to AFI transition increases as the chromium concentration is increased and a higher temperature PM to PI transition appears.

**References**


1. D. McWhan, T. Rice, and J. Remeika, Phys. Rev. Lett. 23 (1969) 1384.
2. D. McWhan, and J. Remeika, Phys. Rev. B. 2 (1970) 3734.
3. M. Nakahira, S. Horichi, and H. Ooshima, J. Appl. Phys. 41 (1970) 836.
4. D. McWhan, and J. Remeika, T. Rice, W. Brinkman, W. Maita, and A. Menth, Phys. Rev. Lett. 27 (1971) 941.
5. D. McWhan, A. Menth, J. Remeika, W. Brinkman, and T. Rice, Phys. Rev. B. 7 (1973) 1920.
6. H. Kuwamoto, J. Honig, and J. Appel, Phys. Rev. B 22 (1980) 2626.
7. S. Shivashankar, J. Honig Phys. Rev. B. 28 (1983) 5695.
8. F. Chudnovski, V. Andreev, V. Kuksenko, V. Piculin, D. Frolov, P. Metcalf, and J. Honig, J. Sol. State Chem. 133 (1997) 430.
9. F. Case, J. Vac. Sci. Technol. A. 9(3) (1991) 461.
10. K. Rogers, J. Coath, and M. Lovell, J. Appl. Phys. 70 (1991) 1412.
11. D. Partow, S. Gurkovich, K. Radford, and L. Denes, J. Appl. Phys. 70 (1991) 443.
12. H. Schuler, S. Klimm, G. Weissmann, C. Renner and S. Horn, Thin Solid Films 299 (1997) 119.
13. I. Yamaguchi, T. Manabe, T. Kumagai, W. Kondo, and S. Mizuta, Thin Solid Films 366 (2000) 294.
14. P. Jin, M. Tazawa, K. Yoshimura, K. Igurashi, S. Tanemura, K. Macak and U. Helmersonn, Thin Solid Films 375 (2000) 128.
15. B. Sass, C. Tusche, W. Felsch, N. Quaas, A. Weismann, and M. Wenderoth, J. Phys. Condens. Matter 16 (2004) 77.

16. C. Muller, A.A. Nateprov, G. Obermeier, M. Klemm, R. Tidecks, A. Wixforth and S. Horn, J. Appl. Phys. 98 (2005) 84111.
17. Q. Guo, D. Kim, S. Street, and D. Goodman, J. Vac. Sci. Technol, A17 (1991) 1887.
18. J. Biener, M. Baumer, R. Madix, P. Liu, E. Nelson, T. Kendelewicz, and G. Brown, Surface Sci. 441 (1999) 1.
19. H. Miyazaki, M. Kamei, and I. Yasui, Thin Solid Films 343-344 (1999) 168.
20. Q. Guo, S. Lee, and D. Goodman, Surface Sci. 437 (1999) 38.
21. P. Jin, M. Tazawa, M. Ikeyana, S.Tanemura, K. Macak, X. Wang, S. Olafsson and U. Hellmersonn, J. Vac. Sci. Technol. 17(4) (1999) 1817.
22. A. Dupuis, M. Haija, B. Richter, H. Kuhlenbeck, and H. Freund, Surface Sci. 539 (2003) 99.
23. Q. Luo, Q. Guo and E.G. Wang, Appl. Phys. Lett. 84, (2004) 2337.
24. S. Yonezawa, Y. Muraoka, Y. Ueda and Z. Hiroi, Sol. State Commun. 129 (2004) 245.
25. J. Schoiswohl, M. Sock, S. Surnev, M. Ramsey, F. Netzer, G. Kresse, and J. Anderson, Surface Sci. 555 (2004) 101.
26. B. Sass, C. Tusche, W. Felsch, F. Bertran, F. Fortuna, P. Ohresser, and G. Krill, Phys .Rev. B. 71 (2005) 014415.
27. F. Pfuner, J. Schoiswohl, M. Sock, S. Surnev, M. Ramsey, and F. Netzer, Condens. Matter 17 (2005) 4035.
28. C. Greenberg and .D. Singleton, Solar Energy Materials 16 (1987) 501.
29. J. Piao, S. Takahasi, and S. Kohiki, Jpn. J. Appl. Phys. 37 (1998) 6519.
30. J. Shepherd and C. Sandberg, Rev. Sci. Instrum. 55 (1984) 1696.

**Figure Captions:**

1. Phase diagram for the metal-insulator transition in single crystal $V_{2-y}O_3$ and $(V_{1-x}Cr_x)_2O_3$ as a function of temperature, on cooling (extracted from references 1 and 6.)
2. PXD patterns of sol-gel derived vanadium oxide films. (a) The x-ray diffraction pattern of a 300 nm thick $V_2O_3$ film deposited on (1120) oriented A- sapphire substrate and (b) (0001) oriented C-sapphire (0001).
3. TEM images of crystallites from a $V_2O_3$ film with the substrate removed (X 150 K).
4. Atomic Force Microscope images of a $V_2O_3$ film deposited on a (0001) sapphire substrate. The images were obtained using non-contact mode. The scan area in image (a) is 1μ x 1μ and that in image (b) is 500 nm x 500 nm.
5. Electrical resistivity versus temperature for $V_2O_3$ films on (a) oriented C- sapphire substrate, and (b) oriented A- sapphire substrate.
6. Optical transmission versus temperature for a $V_2O_3$ film deposited on a (0001) sapphire substrate.
7. Electrical resistivity versus temperature. (a) The electrical resistivity versus temperature for $(V_{1-x}Cr_x)_2O_3$, films on cooling. (b) The electrical resistivity versus temperature for single crystal $(V_{1-x}Cr_x)_2O_3$, on cooling, extracted from reference 6.
8. Optical transmission versus temperature for a $(V_{1-x}Cr_x)_2O_3$ film deposited on a (0001) sapphire substrate.
9. The optical transmission versus temperature for V2-yO3 films deposited on (0001) sapphire and annealed at low oxygen partial pressures in a controlled atmosphere, vertical quench furnace

Figure

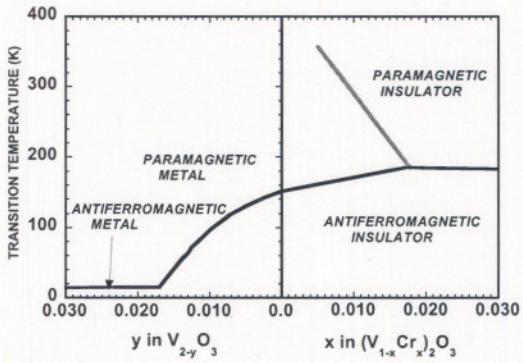
TRANSITION TEMPERATURE (K)
400
300
200
100
0
PARAMAGNETIC
INSULATOR
PARAMAGNETIC
METAL
ANTIFERROMAGNETIC
METAL
ANTIFERROMAGNETIC
INSULATOR
0.030
0.020
0.010
0.0
0.010
0.020
0.030
y in $V_{2-y}O_3$
x in $(V_{1-x}Cr_x)_2O_3$

Figure

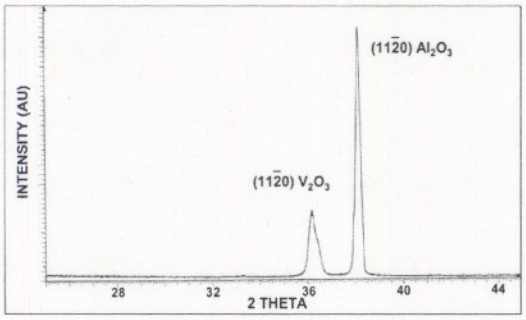
INTENSITY (AU)
(11$\bar{2}$0) $Al_2O_3$
(11$\bar{2}$0) $V_2O_3$
28
32
36
40
44
2 THETA

2a

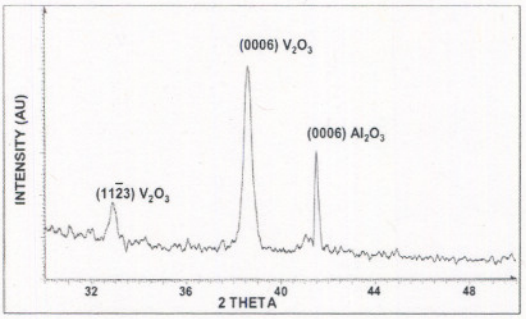
INTENSITY (AU)
(0006) $V_2O_3$
(0006) $Al_2O_3$
(11$\bar{2}$3) $V_2O_3$
32
36
40
44
48
2 THETA

2b

Figure

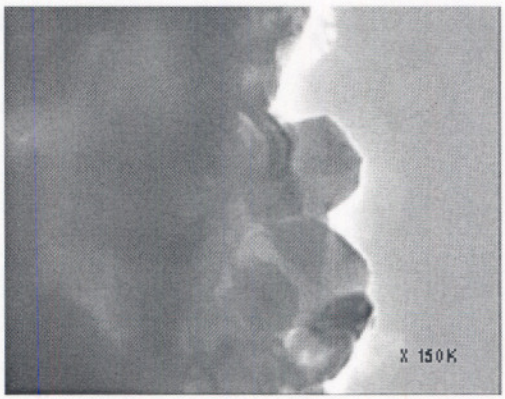

Figure

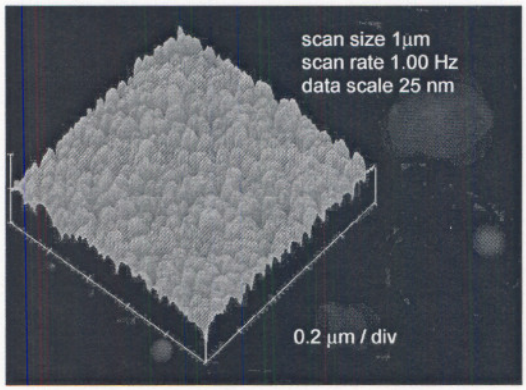
scan size 1µm
scan rate 1.00 Hz
data scale 25 nm
0.2 µm / div

4a

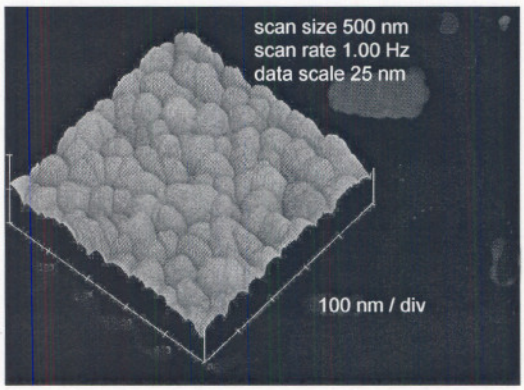
scan size 500 nm
scan rate 1.00 Hz
data scale 25 nm
100 nm / div

4b

Figure

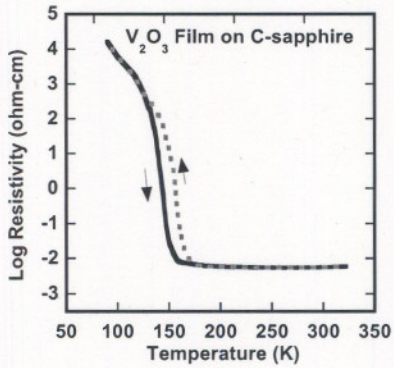


5a

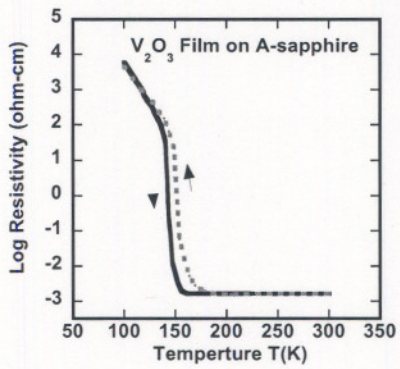


5b

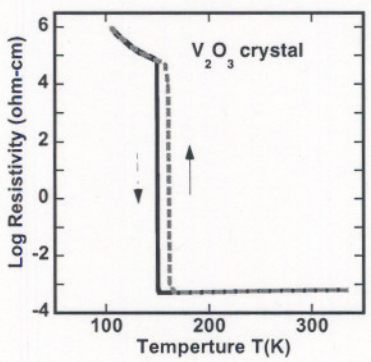


5c

Figure

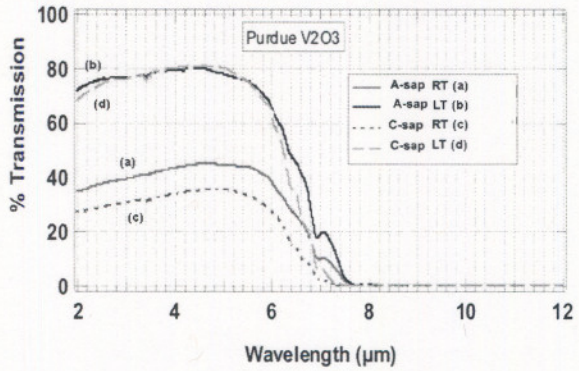
Purdue V2O3
A-sap RT (a)
A-sap LT (b)
C-sap RT (c)
C-sap LT (d)
(a)
(b)
(c)
(d)
% Transmission
Wavelength (μm)
100
80
60
40
20
0
2
4
6
8
10
12

Figure

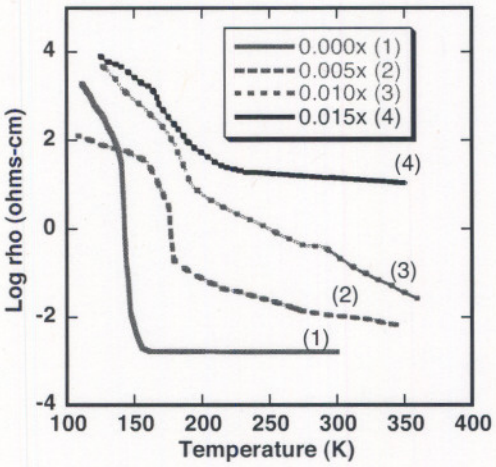
0.000x (1)
0.005x (2)
0.010x (3)
0.015x (4)
(4)
(3)
(2)
(1)
Log rho (ohms-cm)
4
2
0
-2
-4
100
150
200
250
300
350
400
Temperature (K)

7a

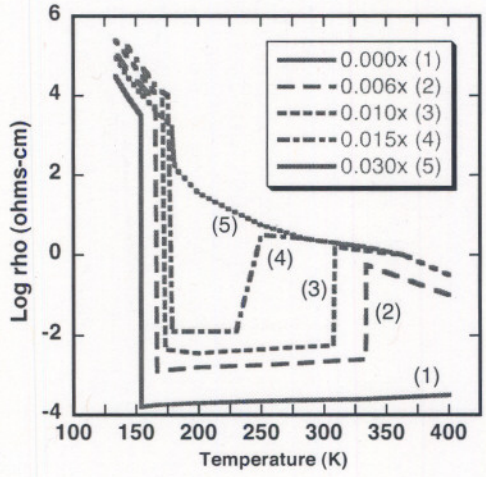
0.000x (1)
0.006x (2)
0.010x (3)
0.015x (4)
0.030x (5)
(5)
(4)
(3)
(2)
(1)
Log rho (ohms-cm)
6
4
2
0
-2
-4
100
150
200
250
300
350
400
Temperature (K)

7b

Figure

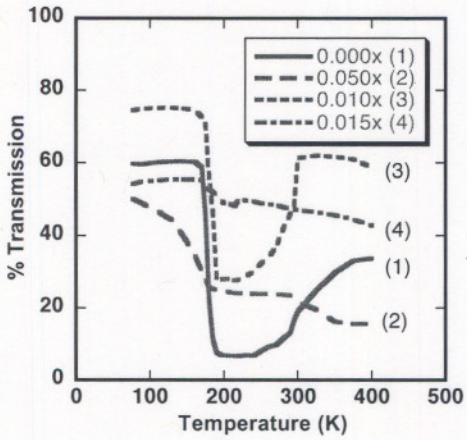
100
80
60
40
20
0
% Transmission
0
100
200
300
400
500
Temperature (K)
0.000x (1)
0.050x (2)
0.010x (3)
0.015x (4)
(3)
(4)
(1)
(2)

Figure

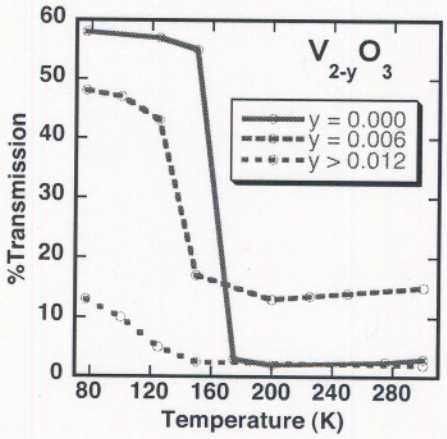
V 2-y O 3
y = 0.000
y = 0.006
y > 0.012
%Transmission
Temperature (K)
0
10
20
30
40
50
60
80
120
160
200
240
280